2D colloids in rotating electric fields: A laboratory of strong tunable three-body interactions

Egor V. Yakovlev[a], Nikita P. Kryuchkov[a], Sofia A. Korsakova[a], Nikita A. Dmitryuk[a], Pavel V. Ovcharov[a], Mihail M. Andronic[a], Ilya A. Rodionov[a,1], Andrei V. Sapelkin[c], Stanislav O. Yurchenko[a,*]

[a] *Bauman Moscow State Technical University, 2nd Baumanskaya street 5, 105005 Moscow, Russia*
[b] *Dukhov Automatics Research Institute (VNIIA), Sushchevskaya street 22, 127055 Moscow, Russia*
[c] *School of Physics and Astronomy, Queen Mary University of London, London E1 4NS, England*

Abstract

Many-body forces play a prominent role in structure and dynamics of matter, but their role is not well understood in many cases due to experimental challenges. Here, we demonstrate that a novel experimental system based on rotating electric fields can be utilised to deliver unprecedented degree of control over many-body interactions between colloidal silica particles in water. We further show that we can decompose interparticle interactions explicitly into the leading terms and study their specific effects on phase behaviour. We found that three-body interactions exert critical influence over the phase diagram domain boundaries, including liquid-gas binodal, critical and triple points. Phase transitions are shown to be reversible and fully controlled by the magnitude of external rotating electric field governing the tunable interactions. Our results demonstrate that colloidal systems in rotating electric fields are a unique laboratory to study the role of many-body interactions in physics of phase transitions and in applications, such as self-assembly, offering exciting opportunities for studying generic phenomena inherent to liquids and solids, from atomic to protein and colloidal systems.

Keywords: Colloids, Tunable interactions, Rotating electric fields, Many-body interactions, Self-assembly, Phase transitions, Phase diagram, Molecular dynamics simulations

1. Introduction

Understanding relationships between interparticle interactions across length scales, from atoms to colloids, their collective dynamics, and emerging collective properties is a challenging problem in fields as diverse as condensed and soft matter, physical chemistry, and materials science. Many-body forces, in particular, widely feature in nature and are known to affect the structure and properties of strongly-coupled atomic [1], molecular [2, 3], colloidal and protein systems [4–8]. Unfortunately, collective phenomena cannot be easily visualised *in situ* on atomic or molecular scale. Molecular dynamics (MD) simulations can offer a viable alternative for examination of relationships between structure, dynamics, transport and thermodynamic properties, and potentials. However, in many cases, simulations are guided and are limited by the interactions derived from the real-life systems, with all the problems [9, 10] of inferring interatomic potentials from the experimental data (e.g. due to the selection of metrics used: pair distribution functions, bulk elastic and dynamic properties etc.). At the same time, exotic potentials can, of course, be used in simulations, but questions arise about their practical implementation (e.g. for the purpose of self-assembly). In this context, an experimental platform capable of delivering systematic control over the many-body (and over the pairwise and three-body parts in particular) interactions, while providing particle-resolved visualisation can offer an opportunity to move beyond widely employed structural metrics, while providing access to observation and control of novel phenomena.

One such platform are colloids that have been known for a long time as model systems exhibiting a wide range of "molecular-like" phenomena [8, 11–14], including crystallisation and melting [15–21], reentrant and solid-solid phase transitions [22–24], condensation and critical phenomena [25–27], molecular-like interactions [28, 29], sublimation [30], gelation and slow dynamics in glasses [31–34]. Furthermore, self-assembly of colloidal materials is attractive for broad range of applications in photonics [35, 36] and 3D printing [37–39]. Naturally, a some efforts have already been made to study colloids with long-range interactions, mostly on the account of their suitability as model systems to investigate phase transitions [27, 40]. However, the systematic effects of many-body interactions in colloids are not well studied as yet. Indeed, a recent study reported in Ref. [41] has suggested that many-body interactions should result in a number of unique and promising structural and

*Corresponding author
Email address: st.yurchenko@mail.ru (Stanislav O. Yurchenko)

dynamic properties. Furthermore, in many such systems the means to control interactions are limited (e.g. by the selection of the host medium and nature of the particles). In cases where sophisticated control can be implemented [42–45], the effect of many body forces have not been investigated and the corresponding theoretical framework to inform the choice of parameters (of for example AC electric fields) is currently lacking. However, it is clear that *rotating electric fields* provide a way to induce and control *long-range* and *many-body tunable interactions* in colloidal systems, whereas collective dynamics can be visualised *in real-time* with the spatial resolution of individual particles.

In rotating fields, the following mechanism governs the tunable interactions in a monolayer colloidal system [46–49]: The external field polarises colloidal particles resulting in anisotropic interactions, but if the field is rotated fast (compared to the time of particle diffusion) in the plane of the system, the interaction attains an isotropic tunable dipolar attraction at large distances [47, 49]. As a consequence, the energy of the colloidal system is completely determined by its instantaneous spatial configuration (i.e., the states become averaged over the fast variables), and can be described by an effective interaction potential [50, 51]. Thus, the states of colloidal system in rotating electric field can be compared to *equilibrium phases* in a system of particles with equivalent pairwise and three-body interactions, whereas the many-body forces of higher orders are negligible [50]. Crucially, the interaction strength is controlled with the magnitude of the applied field and can be tuned *in situ*. A similar approach can, of course, be implemented with rotating magnetic fields [52–59]. Assuming that electric field rotates with frequency that is high compared to the Maxwell relaxation time of the solvent, one can neglect electrokinetic effects and the effects of ionic cloud deformation in the solvent (the Debye-Falkenhagen effect) [11]. Under this assumption, electric and magnetic problems can be described within the static approximation [51].

In recent theoretical studies [50, 51, 60], the tunable interactions in rotating fields were found to be critically dependent on the sign of the dielectric (magnetic) contrast between the particles and the solvent, described by the small parameter $\lambda = (\varepsilon_P - \varepsilon_S)/8(\varepsilon_P + 2\varepsilon_S)$ (here, $\varepsilon_{P,S}$ is the electric (magnetic) permittivity of the particles and the solvent) [51]. At $\lambda < 0$ (silica particles in deionised water in electric fields), the tunable interactions were shown to have (i) a long-range dipolar attraction, (ii) a short-range tunable repulsion, and (iii) expressed three-body interactions in dense clusters [50]. On the other hand, at $\lambda > 0$ (iron oxide particles in water in magnetic fields), there is no short-range tunable repulsion, and three-body interactions are weak. Dependence of the interactions on the λ-sign is a nontrivial effect, caused by a complicated mutual polarisation of particles in rotating fields, while the absolute λ-value is a measure of strength of three-body forces compared to pairwise ones [51]: The magnitude of tunable pairwise interactions is $\propto \lambda^2$, since the particle electric dipole moment is proportional to the Clausius-Mossotti factor (and dielectric contrast). Three-body interactions arise from the change in interaction energy due to additional polarisation of interacting particles by a third particle. This effect is proportional to the dipole of the third particle, $\propto \lambda$, and, hence, the magnitude of three-body forces is $\propto \lambda^3$ in the first order of perturbation theory [51]. As a result, the magnitude of three-body interactions with respect to the pairwise ones can be approximately characterised as $\propto \lambda$. For instance, in the case of silica vs iron oxide particles in water $|\lambda_{SiO_2}/\lambda_{Fe_3O_4}| \simeq 2.2$ (see Materials and Methods) the three-body forces are *enhanced by more than a factor or two*, suggesting that the tunable interactions between the colloids in rotating electric fields can provide unprecedentedly strong three-body part, unavailable in other model systems (including magnetic ones [53–58, 61–64]). However, neither the tunable interactions nor phase transitions in colloids in rotating electric fields have ever been studied.

The pronounced long-range character of tunable interactions in colloids, governed in real time by rotating electric fields, makes these systems a unique tool to study a number of key problems, such as kinetics of condensation and crystallisation, routes of self-assembly of functional materials, diffusion in liquids, formation and roughening of gels, and recrystallisation of polydomain structures. Since the works by Axilrod and Teller [65] and by Barker and Henderson [66], it is known that a correct description of liquids or solids must take into account three-body interactions. However, the specific role of three-body forces in structural and transport phenomena remains unclear for atomic, molecular, colloidal, and crowded protein systems. Another fundamental problem is related to the poorly understood effect of attraction range of interparticle forces, which is known to affect phase diagrams and critical behaviour [67, 68], but remains virtually unstudied experimentally. The tunable dipolar attraction is much more long-range compared to the depletion attraction [25–27]. Due to this, particle-resolved studies with the tunable colloids should allow to understand the role of three-body forces and of the attraction range in phase transitions, thermodynamics, transport, and elastic properties of classical liquids and solids.

In the present paper, we turn to practical implementation of an experimental platform for many-body interactions based on the ideas outlined above. We explicitly decompose many-body (long-range) interactions into two- and three-body leading terms to investigate their corresponding effects. With a novel and original approach, we study the interactions and phase transitions in a monolayer (2D) colloidal system with *in situ* tunable interactions induced by in-plane rotating electric field. Using experiments and MD simulations, we demonstrate that the system constitutes a unique platform for studying the effects of long-range interactions on phase transitions in liquids and solids. Detailed analysis shows sensitivity of interactions to the internal structure of colloidal particles paving

the way towards engineering and tuning their interactions further by altering the structure. For the first time, we measured directly tunable pairwise interactions between particles in rotating electric field, visualised phase transitions, and found that the observed three-body interactions provide a clear analogy with those in charged colloids, serving as a model of globular proteins. The phase diagram is found to be consisting of gaseous, crystalline, fluid, and supercritical domains, resembling that in typical bulk materials. We found that the phase states are strongly affected by three-body forces, especially in the fluid region, wherein the significant change in binodal liquid-gas and the shift of critical point due to three-body forces is revealed for the first time. The results of present paper establish a groundbreaking methodology for future studies by providing a novel experimental platform to study a wide range of fundamental physical phenomena and for application development.

2. Materials and methods

2.1. Details of experiments

To study the interactions and phase diagram of a monolayer colloidal system in rotating electric fields, we performed experiments using methodology and setup developed in Ref. [49]. The setup allows us to tune the interactions between colloidal particles elicited by the in-plane rotating electric field, to study their collective behaviour, phase transitions, and many-body phenomena.

The electrodes were fabricated with two photolithography steps. First, the 2" quartz wafers were cleaned in Piranha solution. For electrode formation, we used a bilayer lift-off process, consisting of 1.0 μm positive photoresist (SPR955-cm 1.4) and 0.5 μm thick coating (LOR 5B) with high dissolution rate in TMAH-based photoresist developer (MF-CD 26), that ensured the bilayer profile undercut. In this case, the sidewall was less coated during metal deposition step. We used direct laser writing for photoresist exposure step. After development, we oxygenised the residual thin resist layer, to achieve good metal adhesion to the substrate. We deposited a 100-nm-layer using high-vacuum electron-beam evaporation method. Further lift-off in hot (NMP-based) solvents removed the bilayer stack along with the material deposited thereon. A similar process we used for lifting-off a 200-nm-thick protective dielectric layer of Al_2O_3.

We used colloidal suspensions of monodisperse silica particles with diameter of $\sigma = 2.12 \pm 0.06$ μm (SiO_2, Microparticles GmbH, Germany) dispersed in deionised water with resistivity of 18.2 M$\Omega \times$ cm (conductivity of 0.055 μS $\times$ cm^{-1}), produced by purification of distilled water with ion-exchanging resins. Due to weak conductivity, the experiments in the field rotating with the frequency 30 kHz can be performed without the direct contact between the chromium lithographic electrodes and the solvent (contactless scheme) [49]. Technical details of our experiments are similar to those reported in Ref. [49], the scheme of experimental cell we used is shown in Fig. S1 [69].

The surfaces of the glass cell were treated with ethanol and deionised water, and dried at temperature of 150°C for 30 minutes. To form a hydrophobic coating, the optical interfaces were then treated by deposition of 3% solution of polymethylsiloxane oil (PMS-200) in cyclohexane and annealed at 250°C for 120 minutes. Then, the suspension was placed into the cell and a colloidal monolayer was sedimented.

Tunable pairwise interactions in rotating electric fields were studied with a dilute suspension of microparticles with a bulk concentration of ~ 0.1 wt%. After the particles were sedimented in the cell, the rotating field was applied. Voltages at the electrodes were oscillating with phase shift to produce electric field rotating in the plane of self-assembly [49]. The field strength was tuned with the magnitude of voltage oscillations at the electrodes in the range $E = (2 \dots 3.5)$ V/mm (that corresponds to $200 - 350$ V at electrodes): in our setup, 100 V at electrodes corresponds to $E_0 \simeq 1.025$ V/mm electric field in the colloidal suspension [49]. The experiments were performed at different, relatively high E-values, to prevent breakdown of particle pairs. We observed a lot of isolated pairs, the distances between them were approximately $(20 \dots 25)$ μm, the motion of particles was recorded with video microscopy and tracked with standard methods. About 300 particles in the dilute suspensions were studied, and 20 experiments were performed at each voltage, providing 10^4 frames to obtain the statistics of distances between the particles.

The phase transitions of the monolayer system were studied experimentally using a dense suspension (bulk concentration was about 1 wt%) with the initial areal density close to the critical one. After the monolayer was sedimented, the field was gradually increased until the particles started to form colloidal drops, followed by their crystallisation. Then, the system was kept for about 15 min, so that the small crystallites began to coalescence. To obtain a monocrystalline cluster, the polycrystals were "annealed": The field magnitude was decreased, and the crystallites were kept for some time so that the defects (dislocations and vacancies) would have moved towards the free surface. Then the field strength was increased to assemble a large crystallite. The measurements were performed during stepwise decrease in the field strength, from $7.5E_0$ to $1.5E_0$. This methodology was used to obtain the domain boundaries on the phase diagram. At each field magnitude, we recorded the videos of clusters, after holding them for $5-30$ minutes (depending on E), to equilibrate the system. Clusters of about 10^3 particles were studied (starting from about 400 particles, bulk phase behaviour is reproduced), 10 experiments were performed at each voltage, and 50 frames were used, to obtain the statistics of Voronoi cells.

The images of the assembled clusters were processed with the method based on the analysis of the distances between the particles in the neighboring Voronoi cells [70]:

The Voronoi cells of particles in condensed clusters have a more regular shape than those corresponding to gas or surface particles. Therefore, the standard deviation of the distances between the particles in neighboring Voronoi cells normalised to their area can be used as an order parameter. Particles with the local order parameter less than the threshold are considered as condensate, surface particles are identified at the interface "gas-condensate" (see [70] for details of the method). As a result, the particles belonging to condensed (liquid or solid) phase, to gas, and at interface were identified, and the gas-condensate binodal was obtained.

Despite using high-frequency fields, a weak rotation of small clusters (duplets and triplets) was observed at the stages of preparation for the experiment. This rotation is assumed to be elicited by rotation of individual particles in the clusters due to a delay between particle polarisation and the external polarising field. However, this effect did not affect the results for dense systems: The experimental measurements were started, once the clusters were large enough to suppress the rotation. The observed rotation of particles, their hydrodynamic interactions, and dynamics of small colloidal clusters are extremely interesting, but stand beyond the scope of present paper and will be considered in a future manuscript.

2.2. Details of MD simulations

To compliment our experiments and to reveal the role of three-body forces versus purely pairwise interactions, we performed molecular dynamic (MD) simulations of a monolayer system of particles with the interaction energy

$$\begin{aligned} U &= U_0 + \epsilon U_{\rm tun}, \qquad U_0 = \sum_{\alpha<\beta} \varphi_0(r_{\alpha\beta}), \\ U_{\rm tun} &= \sum_{\alpha<\beta} \varphi_{\rm tun}(r_{\alpha\beta}) + \sum_{\alpha<\beta<\gamma} F(\mathbf{r}_\alpha, \mathbf{r}_\beta, \mathbf{r}_\gamma), \end{aligned} \tag{1}$$

where U_0 and $U_{\rm tun}$ are the basic (without the external rotating field) and tunable parts of the interaction, ϵ is the tunable interaction magnitude, and $\mathbf{r}_{\alpha\beta} = \mathbf{r}_\beta - \mathbf{r}_\alpha$.

Similarly to Ref. [71], the $\varphi_0(r)$ was assumed to be hard sphere with short-range Yukawa repulsion

$$\beta\varphi_0(r) = \begin{cases} \infty, & r/\sigma < 1; \\ \beta\epsilon_Y \dfrac{\exp\left[-\kappa\sigma(r/\sigma-1)\right]}{r/\sigma}, & r/\sigma > 1, \end{cases} \tag{2}$$

where σ is the hard-sphere particle diameter, $\kappa = 1/\lambda_D$ is the inverse screening (Debye) length, and we used $\beta\epsilon_Y = 1$. For silica particles in deionised water, under the same experimental conditions as we had, $\kappa\sigma = \sigma/\lambda_D \approx 25.8$, as was obtained in Ref. [72].

The magnitude ϵ of the tunable interaction for bulk particles was shown in Ref. [51] to be

$$\epsilon = \lambda^2(1-8\lambda)\sigma_p^3 E^2, \quad \lambda = \frac{1}{8}\frac{\varepsilon_P - \varepsilon_S}{\varepsilon_P + 2\varepsilon_S}, \tag{3}$$

where ε_P and ε_S are the relative dielectric permittivities of particle and the solvent, E is the magnitude of a uniform rotating electric field in the solvent, and σ_p is *the effective polarisation diameter* of the particle – the only free parameter of theory, which is unknown *a priori*, but can be obtained from experiment (see Eq. (12) and discussion).

The tunable interaction $U_{\rm tun}$ consists of pairwise and three-body terms, whereas the higher order effects were shown in Ref. [50] to be negligible. We used the pairwise potential [60]

$$\varphi_{\rm tun}(r) = -\frac{1}{(r/\sigma_p)^3}\left(1 + \frac{15\lambda p_1^{(2)}}{2(r/\sigma_p)^3} + \frac{14\lambda^2 p_2^{(2)}}{(r/\sigma_p)^6}\right) \tag{4}$$

with parameters $p_1^{(2)} = 0.945$ and $p_2^{(2)} = -10.49$ calculated in Ref. [60]. One can see that, in addition to the dipolar term, the pairwise interactions include the terms of higher orders, caused by mutual repolarisation of particles and corresponding multipoles of higher orders [51, 60].

The fit for three-body energy of the interactions $F_{\alpha\beta\gamma} \equiv F(\mathbf{r}_\alpha, \mathbf{r}_\beta, \mathbf{r}_\gamma)$ was used in the form [51, 60]

$$F_{\alpha\beta\gamma} = F^{(3)}_{\alpha\beta\gamma} + F^{(4,1)}_{\alpha\beta\gamma} + F^{(4,2)}_{\alpha\beta\gamma}, \tag{5}$$

with the terms

$$\begin{aligned} F^{(3)}_{\alpha\beta\gamma} &= -6\lambda\sigma_p^6\left(\frac{C_3(\phi_\alpha)}{r^3_{\alpha\beta}r^3_{\alpha\gamma}} + \frac{C_3(\phi_\beta)}{r^3_{\alpha\beta}r^3_{\beta\gamma}} + \frac{C_3(\phi_\gamma)}{r^3_{\alpha\gamma}r^3_{\beta\gamma}}\right), \\ F^{(4,1)}_{\alpha\beta\gamma} &= -6\lambda^2\sigma_p^9\left[\frac{C_{4,1}(\phi_\alpha)}{r^3_{\alpha\beta}r^3_{\alpha\gamma}}\left(\frac{1}{r^3_{\alpha\beta}} + \frac{1}{r^3_{\alpha\gamma}}\right) + \right. \\ &\quad \left. + \frac{C_{4,1}(\phi_\beta)}{r^3_{\alpha\beta}r^3_{\beta\gamma}}\left(\frac{1}{r^3_{\alpha\beta}} + \frac{1}{r^3_{\beta\gamma}}\right) + \frac{C_{4,1}(\phi_\gamma)}{r^3_{\alpha\gamma}r^3_{\beta\gamma}}\left(\frac{1}{r^3_{\alpha\gamma}} + \frac{1}{r^3_{\beta\gamma}}\right)\right], \\ F^{(4,2)}_{\alpha\beta\gamma} &= -24\lambda^2\sigma_p^9\frac{C_{4,2}(\phi_\alpha,\phi_\beta,\phi_\gamma)}{r^3_{\alpha\beta}r^3_{\beta\gamma}r^3_{\alpha\gamma}}, \end{aligned} \tag{6}$$

where $\cos\phi_\alpha = (\mathbf{r}_{\alpha\beta}\cdot\mathbf{r}_{\alpha\gamma})/(r_{\alpha\beta}r_{\alpha\gamma})$. The amplitude functions C_3, $C_{4,1}$, and $C_{4,2}$ are:

$$\begin{aligned} C_3 &= \frac{1}{2}(p_1^{(3)} + 9p_2^{(3)}\cos 2\phi), \\ C_{4,1} &= \frac{1}{2}(5p_3^{(3)} + 9p_4^{(3)}\cos 2\phi), \\ C_{4,2} &= -(2p_5^{(3)} + 9p_6^{(3)}\cos\phi_\alpha\cos\phi_\beta\cos\phi_\gamma), \end{aligned} \tag{7}$$

where we used the parameters $p_1^{(3)} = 0.1447$, $p_2^{(3)} = 0.4058$, $p_3^{(3)} = 12.641$, $p_4^{(3)} = 4.3541$, $p_5^{(3)} = 17.246$, $p_6^{(3)} = -19.705$. The parameters were calculated with fitting the data from Ref. [50] by Eqs. (4)-(7), as reported in Refs. [51, 60]. The superscript indices in Eq. (13) are related to different polarisation mechanisms contributing to the tunable three-body potential [60]: $F^{(3)}_{\alpha\beta\gamma}$ is the interaction between a couple of particles mediated by a third particle; $F^{(4,1)}_{\alpha\beta\gamma}$ is due to a more complicated process related to re-polarisation

of a particle; the last term in (5), $F^{(4,2)}_{\alpha\beta\gamma}$ is provided by three-particle interactions with mutual polarisation, similar to Axilrod-Teller energy in theory of molecular forces [51, 59, 60, 65]. Comparing Eqs. (4)-(6), we see that the particular value of λ characterises the relative contribution provided by three-body interactions regarding to the pairwise ones.

The small parameter λ is related to the Clausius-Mossotti factor: in our case its value is $\lambda_{SiO_2} = -5.91 \times 10^{-2}$, since we assume that $\varepsilon_P = 2.97$ for silicon dioxide with 75% porocity, $\varepsilon_S = 80.1$ for deionised water. For comparison, in magnetic suspensions of iron oxide particles in deionised water, $\lambda_{Fe_3O_4} = 2.68 \times 10^{-2}$ ($\mu_P = 1.82$ for iron oxide and $\mu_S = 1$ for water). Therefore, we obtain $|\lambda_{SiO_2}/\lambda_{Fe_3O_4}| \simeq 2.2$

With MD simulations, we considered a 2D system consisting of $N = 931$ particles with unity mass $m = 1$ in a square simulation domain with the sizes $57\sigma \times 57\sigma$ and periodic boundary conditions in Langevin thermostat with temperature $T = 1$ (in energy units). We used the cut-off radius of 15σ and 5σ for the pairwise and three-body terms, respectively. The initial state of the system was set as a round cluster with a hexagonal lattice and distance σ between the neighboring particles. Large magnitude ϵ was chosen at the simulation onset, to stabilise the initial configuration. Then, ϵ was gradually decreased to zero, to reproduce our experimental manipulations.

To reveal the role of three-body interactions in phase states of the system, we performed equivalent MD simulations for three-body and pairwise interacting system, processed the results in the same manner, and compared them. All simulations were performed for 1.6×10^6 simulation steps with timestep $\Delta t = 2.5 \times 10^{-3}\sqrt{m\sigma^2/\beta\epsilon_Y}$ with LAMMPS. The obtained data describing evolution of the cluster were analysed with the phase identification method proposed in Ref. [70], to calculate gas-condensate binodal. The phase identification method was shown in Ref. [70] to provide the same results as the previously-known methods [73]. Furthermore, it allows to obtain binodal "gas-condensate" using cluster analysis, in the same manner for both experiments and MD simulations.

3. Results and discussions

3.1. The pairwise tunable interactions

To recover the *pairwise* tunable interaction potential, we analysed the experimental pair distributions of the distances between particles in dilute suspension of silica particles in deionised water at different magnitudes E of rotating electric field (see details in Materials and Methods). A typical example of an isolated colloidal pair and the corresponding distribution of the distances $w(r)$ at $E = 3E_0 \simeq 3$ V/mm (E_0 is the field corresponding to 100 V at the electrodes) are shown in Figs. 1(a) and 1(b), respectively. With processing of experimental videos, we obtained analogous distributions $w(r, E)$ at different E.

The distribution $w(r)$ for a pair of colloidal particles is related to the pairwise potential as

$$w(r) = A \exp\left(-\frac{\varphi(r)}{k_B T}\right), \quad \varphi(r) = \varphi_0(r) + \epsilon\varphi_{\text{tun}}(r), \quad (8)$$

where $\varphi(r)$ is the total pairwise potential, $\varphi_0(r)$ and $\varphi_{\text{tun}}(r)$ are the basic (without the external field) and tunable parts of the interactions, respectively, ϵ is the magnitude of tunable interaction, k_B and T are the Boltzmann constant and solvent temperature, and A is the normalising constant. With analysis of the distributions $w(r, E)$, the basic and tunable parts of the interactions were reconstructed in two steps as follows.

First of all, since the basic interactions are negligible at large distances, where only the dipolar attraction $\varphi_{\text{tun}}(r) \propto -(\sigma/r)^3$ operates [51], we can rewrite (8) at different E as

$$\ln w(r, E) = -\frac{U_\infty(E)}{k_B T} \cdot \left(\frac{\sigma}{r}\right)^3 + \ln A(E), \quad (9)$$

where we have introduced the normalised magnitude $U_\infty(E)/k_BT$ of the long-range dipolar attraction. Fitting the experimental data for $w(r, E)$ within $2 < r/\sigma < 3.8$ with Eq. (9), we obtained $A(E)$ and $U_\infty(E)/k_BT$. The results for U_∞/k_BT are shown in the inset in Fig. 1(c). We see that U_∞ is indeed proportional to the field squared (see the solid red line in Fig. 1(c)) with $U_\infty(E)/k_BT = \alpha(E/E_0)^2$ and $\alpha \simeq 0.73$. The total pairwise potentials at different E were calculated as

$$\varphi(r, E)/U_\infty(E) = -\ln(w(r, E)/A(E)) \times k_BT/U_\infty(E),$$

and the results are shown in Fig. 1(c) with symbols, whereas the solid black line is the (long-range) dipolar attraction. One can see that the attraction is indeed dipolar for $r/\sigma > 2$, but deviates at small distances.

As the second step, we should accurately separate the (as yet unknown) basic and tunable parts of the interactions, using the known dependencies $A(E)$ and $U_\infty(E)/k_BT$. Considering that $U_\infty(E) \propto E^2$, we may rewrite the total potential as $\varphi(r) = \varphi_0(r) + (E/E_0)^2\varphi_{\text{tun}}(r)$, where we renormalised $\varphi_{\text{tun}}(r)$, writing $(E/E_0)^2$ instead of ϵ, to present the results in the experimentally-convenient terms:

$$-\ln\left(\frac{w(r, E)}{A(E)}\right) = \frac{\varphi_0(r)}{k_BT} + \frac{\varphi_{\text{tun}}(r)}{k_BT}\left(\frac{E}{E_0}\right)^2. \quad (10)$$

Now, the k_BT-normalised potentials $\varphi_0(r)/k_BT$ and $\varphi_{\text{tun}}(r)/k_BT$ at different distances r play the role of parameters in the linear dependence (10) of obtained experimentally $\ln(w(r, E)/A(E))$ as a function of $(E/E_0)^2$. Consequently, we obtained the normalised potentials with the linear fitting of the experimental data, and the results are shown by the symbols in Figs. 1(d) and 1(e). The blue gradient zones in Figs. 1(c)-1(e) correspond to the range of nonlinear screening (a few Debye lengths $\lambda_D \simeq 80$ nm, at $\sigma/\lambda_D \simeq 25.8$ inherent to our experiment [72], the errors

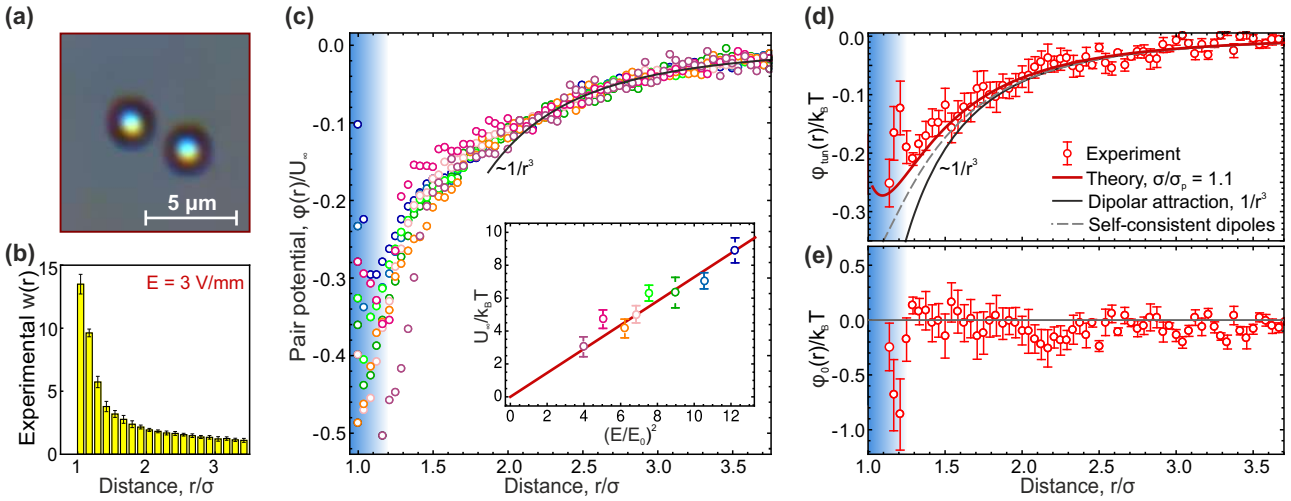

Figure 1: **Tunable pairwise interactions in colloids in rotating electric fields**: (a) an example of a particle couple snapshot (b) the distribution $w(r)$ at $E \simeq 3$ V/mm magnitude of rotating electric field in the suspension. (c) normalised pairwise potential $\varphi(r)/U_\infty$, solid black line is the long-range $1/r^3$-attraction, whereas the magnitude $U_\infty(E)/k_BT$ is shown in the inset. The symbols are coloured in accordance to the field magnitude E, the solid red line is $U_\infty(E)/k_BT = \alpha(E/E_0)^2$ with $\alpha \simeq 0.73$. (d) and (e) the tunable and basic parts of the pairwise potential, symbols are experimentally-obtained values, whereas the lines in (d) are theoretical potential (11) (solid red), dipolar asymptotic (solid black), and the interaction given by the self-consistent dipole model (dashed gray) [50].

of particle tracking are also more pronounced at small distances).

Now, we can compare the experimental results for $\varphi_{\rm tun}(r)/k_BT$ shown in Fig. 1(d) with theoretical potential calculated for silica particles in deionised water in rotating electric field [51, 60]:

$$\frac{\varphi_{\rm tun}(r)}{k_BT} = -\frac{\Gamma}{(r/\sigma_p)^3}\left(1 + \frac{15\lambda p_1^{(2)}}{2(r/\sigma_p)^3} + \frac{14\lambda^2 p_2^{(2)}}{(r/\sigma_p)^6}\right), \quad (11)$$

where $\lambda = 5.91 \times 10^{-2}$, $p_1^{(2)} = 0.945$, $p_2^{(2)} = -10.49$ [60], and $\Gamma = \lambda^2(1-8\lambda)\sigma_p^3 E_0^2/k_BT$ is the magnitude of interaction between particles.

Here, one should make a note regarding the mapping of real particles onto *bulk spheres* via the tunable interactions in rotating electric field. This problem is similar to the mapping of hard-sphere interactions to the real ones, known for a long time, and is strongly dependent on the particular way of measurement of particle diameter [74]: Different methods provide different effective "hard-sphere" diameters. In our case, the tunable interactions are provided by the bulk polarisation of the particles and therefore the interactions are sensitive to the internal structure of particles [75]. The real particles can be porous and partially filled with the solvent, providing an inhomogeneous spatial distribution of the electrostatic properties inside the particle. Therefore, when we speak about *the effective polarisation diameter* σ_p, we mean the diameter of homogeneous particles providing a tunable interaction *equivalent* to that between the real particles. Thus, being determined by the (actually unknown in details) internal structure of the interacting particle, the effective polarisation diameter does not have to be the same as the geometric ("hard-sphere") one, σ. Therefore, equating the

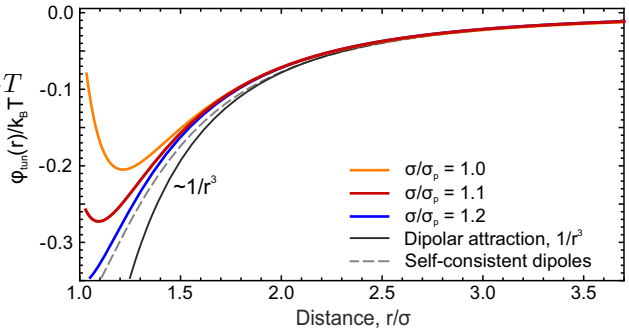

Figure 2: **Tunable pairwise potentials at different effective polarisation diameters of particles**: The curves demonstrate the potential (11) at $\sigma/\sigma_p = 1.0$, 1.1, and 1.2. The dashed grey line is given by self-consistent dipole model, whereas the solid black line is the long-range dipolar asymptotic.

asymptotic dipolar behaviour (9) to that of (11) and taking into account the results for $U_\infty(E)/k_BT$, we derive the polarisation diameter

$$\sigma_p = \left(\frac{\alpha\sigma^3 k_BT}{\lambda^2(1-8\lambda)E_0^2}\right)^{1/6}, \quad (12)$$

from where we obtain $\sigma/\sigma_p = 1.1$ for our system.

Theoretical potential (11) with $\sigma/\sigma_p = 1.1$ is shown in Fig. 1(d) by the solid red line, demonstrating an excellent agreement with experiments. Here, the solid black line is dipolar asymptotic, whereas the dashed grey line is given by the self-consistent dipole model [50]. To further illustrate the evolution of tunable interactions with the change in σ_p, we presented the potential (11) at different ratios $\sigma/\sigma_p = 1.0$, 1.1, and 1.2 in Fig. 2. The solid red, solid black, and dashed grey lines here are the same as those in Fig. 1(d). One can see that, with decrease in σ_p, the in-

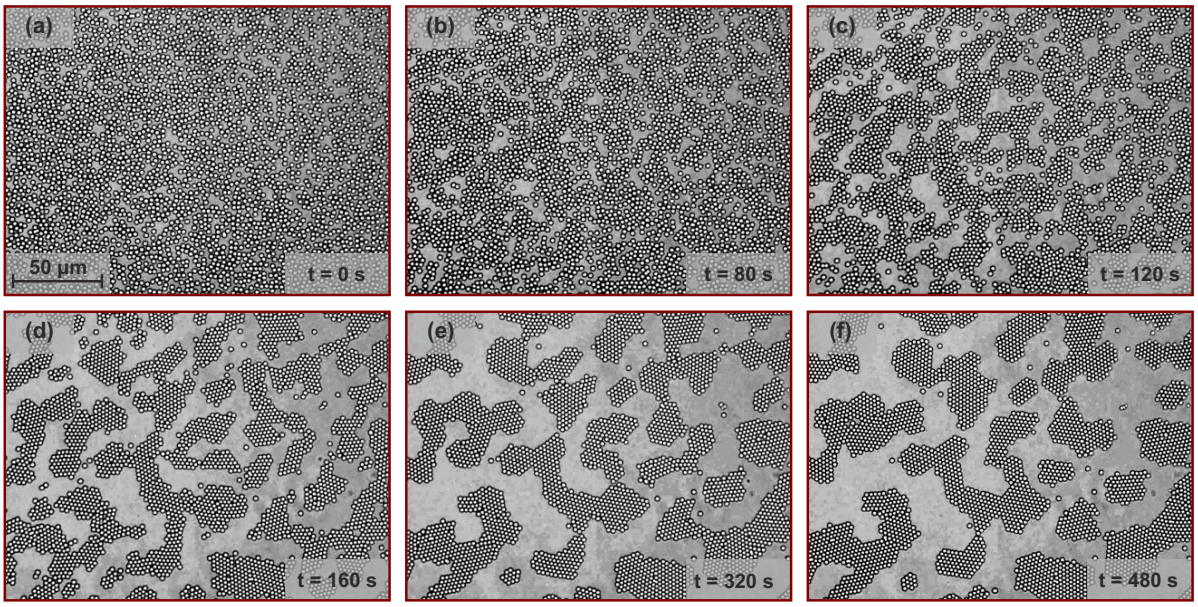

Figure 3: **Spinodal decomposition of colloidal suspension induced by external rotating electric field**: (a)-(f) the shapshots of the suspension at different time moments shown in bottom right corners of the panels. The initially homogeneous state (a) is being decomposed, that is accompanied by formation of "liquid" droplets as shown in (b) and (c) followed by their crystallisation and consequent coarsening illustrated in panels (d)-(f). See Supplemental Movie 1 [69].

teractions become more point-dipolar-like, and the short-range repulsive part vanishes. However, we discovered that the interactions at the given λ are determined *only by the parameter* α (related to σ_p), which can be measured simply with analysis of the long-range dipolar asymptotic (9) in experiments. Moreover, σ_p turns out to be *the only free parameter* of the theory, determining completely the tunable pairwise (and three-body) forces. The significance of this result is that we can reconstruct the tunable interaction potential with simple experimental observations, and without study of internal structure of particles (that is typically difficult or even impossible in experiments).

Since tunable interactions are realised through particle *bulk* polarisation, an important role is played by the contrast in dielectric permittivities of the particle and solvent, or, equivalently, by the sign of λ-parameter [51]. The potential (11) represents a power expansion in λ-series, where the term $\propto 1/r^9$ is positive, providing *the tunable repulsion* at short distances, clearly seen in Fig. 1(d). We see that the tunable interactions are essentially more long-range, compared to those provided by depletion forces: We have the dipolar attraction $\varphi \propto -1/r^3$ versus $\varphi \propto -1/r^9$ reported in Ref. [27], and the energy change at $r/\sigma \simeq 3.5$ in our case corresponds to $r/\sigma \simeq 1.4$ observed in Ref. [27]. Due to this, the coexistence line of liquid and gas is stable [67], and mean-field critical behaviour is expected in vicinity of the critical point "gas-liquid" [68, 70]. The mentioned short-range repulsive term observed in our case (related to the positive $1/r^9$-term) stands in drastic contrast to the tunable magnetic interactions [54, 57, 58], where the attraction increases monotonously with the drop in the distance between particles [50, 51].

The largest difference between the self-consistent dipolar behaviour and the real tunable interactions in Fig. 1(d) is observed at small distances, where the effects of mutual particle polarisation are especially pronounced [51]. Actually, the same polarisation mechanism is responsible for three-body interactions, leading to the strongest effects of three-body forces in our system, that are also inherent to the long-range interactions in dense (liquid and solid) states.

3.2. Phase states and strong tunable three-body forces

Having obtained the pairwise potential, we can now visualise phase transitions and compare the phase states observed experimentally and with MD simulations. To do this, we used dense colloidal suspensions of silica particles in deionised water (see details in Materials and Methods). The rotating electric field was applied to the system, to induce attraction between particles and their "condensation" into colloidal clusters.

A visualisation of how a homogeneous "fluid" colloidal monolayer with near-critical areal density undergoes spinodal decomposition under strong tunable attraction is provided in Fig. 3. Under the applied rotating electric field, the initially homogeneous suspension shown in Fig. 3(a) is being decomposed into "condensed" colloidal clusters and rare ("gaseous") particles, as illustrated in Figs. 3(b) and 3(c). The worm-like structure of solidified clusters with developed boundaries and their coarsening are highlighted in Figs. 3(d)-3(f). Moreover, coexisting liquid and gaseous clusters, typically difficult to observe in systems with short-range attraction, are easily obtained in our experiments.

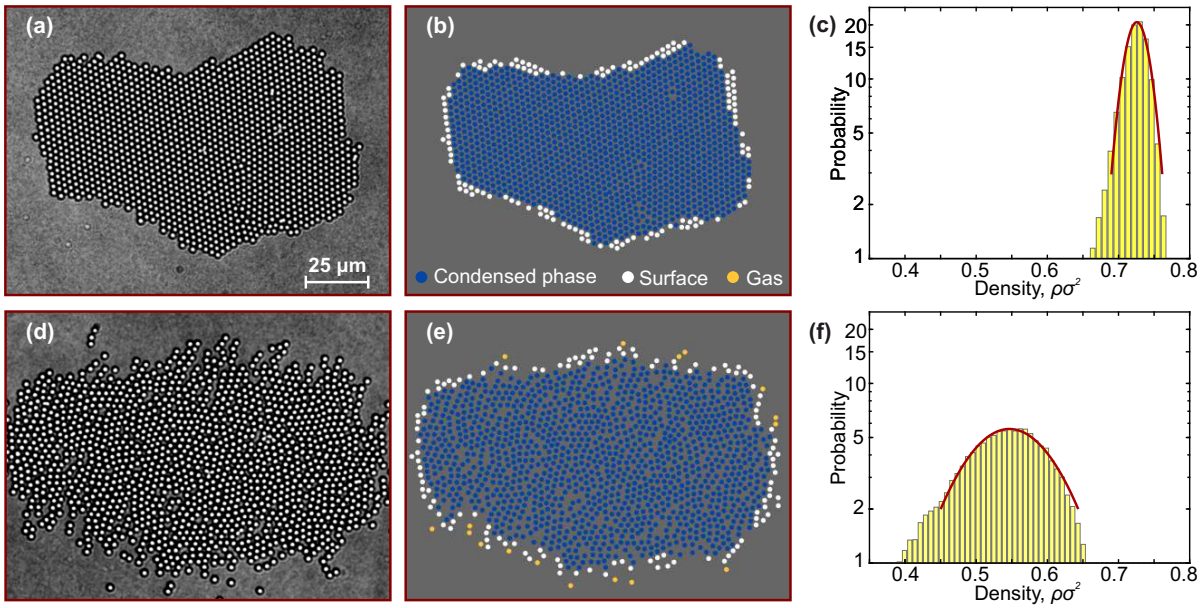

Figure 4: **A colloidal cluster in crystalline and liquid states**: (a) the snapshot of a crystalline cluster consisted of about 1500 particles, (b) an example of particle identification, (c) the distribution of the density (inverse area of Voronoi cells) in the system, histograms are experimental results, red line is the gaussian fit (13), (d)-(f) results for the same cluster in liquid state.

A large colloidal cluster consisting of about 1500 particles in crystalline and liquid states is shown in Figs. 4(a) and 4(d). Particles in gas and condensed state, illustrated in Figs. 4(b) and 4(e), were identified with the method based on the analysis of the distances between particles in neighboring Voronoi cells [70]. Note that one can clearly see a few dislocations inside the crystallite shown in Fig. 4(b), that opens a way, e.g., for future study of their mobility depending on the magnitude of attraction. We note that these rare defects did not affect the overall density distribution in the clusters we studied.

The statistics of the inverse areas (densities) of Voronoi cells for particles in condensate is illustrated in Figs. 4(c) and 4(f). Here, the histograms are experimental results, whereas the red lines are the Gaussian fits (near the distribution maxima)

$$P \propto \exp\left[-K(\rho-\rho_c)^2/2\right], \tag{13}$$

where ρ_c is the average density of the condensate, and parameter K characterises density fluctuations of Voronoi cells.

Following analysis of all experimental videos at different magnitudes of tunable interactions, we constructed the phase diagram in the effective temperature-density coordinates. We normalised the effective temperatures $\widetilde{T} = k_B T/U_\infty(E)$ to their values $\widetilde{T}_{TP}$ at the triple points (TP). We found the triple points in the experiment and simulations using clearly seen drop in the condensed cluster density and parameter K, as shown in Figs. 5(a) and 5(b). The critical point (CP) position was obtained by fitting the gas-liquid binodal with the following parabolic fit near the vertex [70]:

$$\begin{aligned} \rho_l - \rho_g &\simeq B\left(\widetilde{T}_{\rm CP} - \widetilde{T}\right)^{1/2}, \\ \frac{\rho_l + \rho_g}{2} &\simeq \rho_{\rm CP} + b\left(\widetilde{T}_{\rm CP} - \widetilde{T}\right), \end{aligned} \tag{14}$$

where ρ_l and ρ_g are the densities of the liquid and gaseous phase, $\widetilde{T}_{\rm CP}$ and $\rho_{\rm CP}$ are the effective temperature and density at the critical point, B and b are free parameters. The critical exponent 1/2 is used here, because of, in the case of the long-range attraction $\propto -1/r^3$, the 2D system exhibits classical critical behaviour [68]. For MD simulations, we used theoretical pairwise potential with the effective polarisation diameter ($\sigma/\sigma_p = 1.1$) (see details of simulations in Materials and Methods).

The results are shown in Fig. 5(a), where experimental points are shown with red symbols (see Fig. S3 in [69] for experimental points with error-bars). Grey triangles and lines in Fig. 5(a) depict the phase diagram of hard discs with isotropic dipolar attraction, reported in Ref. [71]. The results for parameter K of the fit (13) observed on the crystalline and liquid branches of the gas-condensate line of coexistence are shown in Fig. 5(b). Here, we see that K expectedly drops with increase in effective temperature $\widetilde{T}$, due to the growth of the density fluctuations. The snapshots of the system in crystalline, fluid, and gaseous states, marked by the stars A-F in Fig. 5(a), are presented in Fig. 5(c). The binodal (14) is shown in Fig. 5(a) with the solid red line. Note that this stands in contrast to the depletion attraction used in Ref. [27], which behaves as $\propto -1/r^9$, and, thus, should exhibit 2D Ising class of universality [68]. The unexpected results here is that the line (14) of liquid-gas coexistence is discovered to work

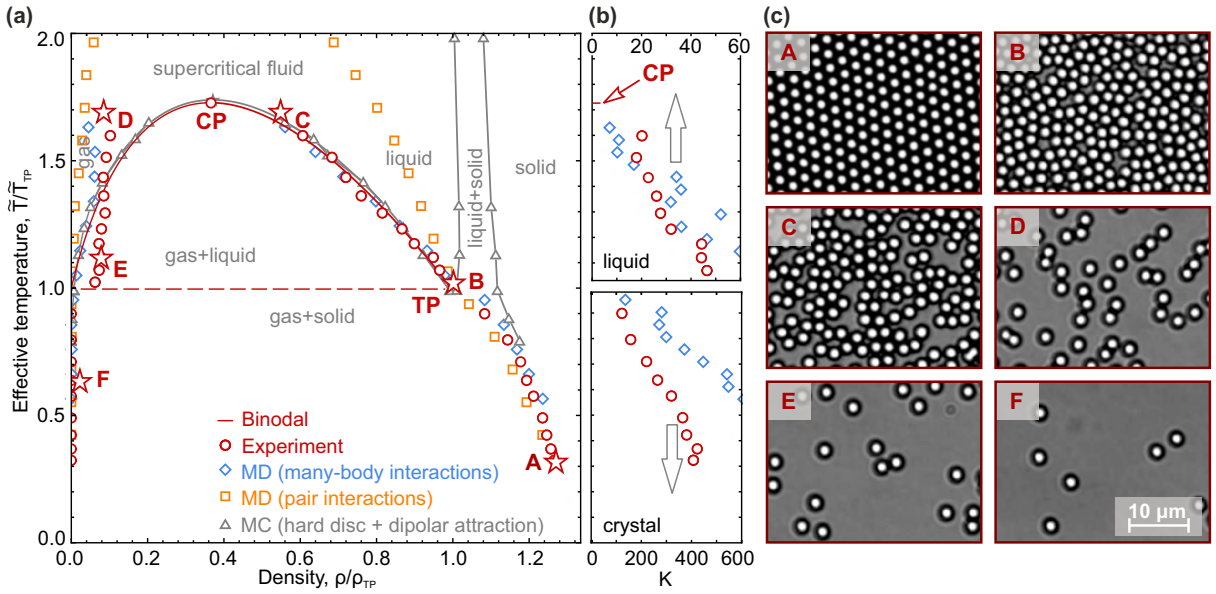

Figure 5: **Phase diagram of colloidal suspension with tunable interactions in rotating electric field**: (a) phase diagram with the critical and triple points (CP, TP), binodal (14) is shown with red solid line for experiment and with solid gray line for system of hard discs with tunable dipolar attraction [71]; (b) parameter K characterising fluctuations of the Voronoi cells' densities in crystalline and liquid clusters; the vertical scale of is the same as in (a), the points are shown in different K-scales (indicated with the arrows) inherent to crystalline and liquid states; (c) the snapshots of the typical crystalline, liquid, and gaseous states of the colloidal system in different points A-F shown at the phase diagram. See Supplemental Movie 2 [69].

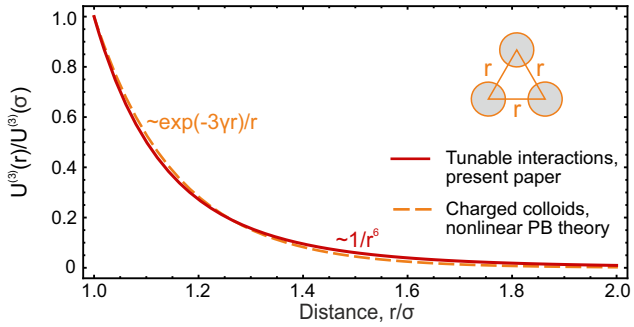

Figure 6: **The mapping of three-body tunable interactions to three-body energy in charged colloidal particles**: The solid red line is the profile of tunable three-body energy of triangular triplet (shown sketchily) in our system at $\sigma/\sigma_p = 1.1$. The dashed orange line is the fit of the three-body interaction in rotating electric field by the energy of triplet calculated within nonlinear Poisson-Boltzmann (PB) theory [4], at $\gamma\sigma \simeq 1.8$ corresponding to the screening $\sigma/\lambda_D \simeq 2.5$).

excellently, from triple to critical point. Note that the discrepancies between experimental and MD results on the gas binodal in Fig. 5(a) are related to the slow relaxation of the gas state in experiment due to Brownian dynamics of individual particles. However, overall, the most striking observation in Fig. 5(a) is a clear discrepancy between the experimental data (red circles) and the MD simulations (orange squares) based on the pair interactions only extracted by the methodology described in Sec. 3.1.

The correspondence between experimental data and MD simulations is increased drastically and becomes excellent once the three-body interactions are included in simulations (blue diamonds). The results shown in Fig. 5(a) shed light onto the role of many-body forces in our system and resolve a paradoxical situation: If we use *only* the pairwise potential (11), derived from the experiment in Fig. 1(d), we obtain wrong phase states (see the difference between the orange and red squares in Fig. 5(a)). Thus, we conclude that interactions and phase states can be explained in consistent manner only by taking into account many-body forces (whose profile is determined with the already known σ_p). Ultimately, the excellent agreement between experiments and theoretical results in Figs. 1(d) and 5(a) reveals that three-body forces play *a crucial role* in the tunable interactions and in phase states in our system.

Another surprising finding is that the liquid-gas binodal can be mapped onto the phase diagram of hard disks with pairwise dipolar attraction [71], as shown in Fig. 5(a) by grey symbols. The observed mapping of our experimental phase diagram to that of hard disks with dipolar attraction [71] along the liquid-gas binodal is likely caused by the following reasons: (i) the three-body interaction contributes to the attraction between particles in clusters [51]; (ii) the particles in a large cluster being "compressed" by the long-range attraction and move close to each other, with their behaviour determined by the hard-sphere repulsion. In small clusters, one may expect that this compression will be weak, thus, providing the basis for size effects in melting and dislocation dynamics, as well as the change in scenario of 2D melting, deserving a separate study in future. Moreover, there is no any proofs that the similarity in phase behaviour provides a similarity, e.g., in diffusion

or elastic properties, and we leave these problem for future investigations.

As we mentioned previously, many-body interactions are inherent to real materials, molecular, colloidal, and protein systems, but their role, e.g., in transport and elastic properties, remains largely unclear. The effects of three-body interactions, studied primarily in charged colloidal (Yukawa) systems with the large screening length, were shown to be significant already at $\sigma/\lambda_D \lesssim 4$ [4–6]. That condition has restricted the particle size and solvents in suspensions suitable for analysis of the effects of many-body interactions. In our experiments $\sigma/\lambda_D \simeq 25.8$, but the characteristic scale of three-body forces is always determined by the effective polarisation diameter σ_p rather than the screening length in the solvent. By examining behaviour of our system, we discovered that we can map the three-body interactions in our system onto those in charged colloids (playing a role of model system for globular proteins [8]). To illustrate it, we present in Fig. 6 the normalised three-body energy $U^{(3)}(r)/U^{(3)}(\sigma)$ for colloidal triplets in our system (at $\sigma/\sigma_p = 1.1$, solid red line, $U^{(3)}(r) = F(\mathbf{r}_\alpha, \mathbf{r}_\beta, \mathbf{r}_\gamma)$ is three-body energy of a regular triangle) and in a charged colloidal system (dashed orange line). The latter was obtained within nonlinear Poission-Boltzmann (PB) theory in Ref. [4], and behaves as $U^{(3)}(r) \propto \exp(-3\gamma r)/r$. Both potentials are negative (that means that three-body forces facilitate compression of a cluster in our case and in the case of charged colloids), and agree remarkably at $\gamma\sigma \simeq 1.8$, as seen in Fig. 6. In charged colloids, this would correspond to the screening parameter $\sigma/\lambda_D \simeq 2.5$ [4]. This fruitful analogy offers rich opportunities for studies of fundamental properties of, e.g., globular proteins, with our model system, wherein the forces can be designed with the particle internal structure and tuned in real time with rotating electric field, offering *unparalleled flexibility*.

4. Conclusions

In this Article, we presented an experimental colloidal model system we have developed, with rich capabilities for *in situ* particle-resolved studies and visualisation of collective behaviour, while offering unprecedentedly strong tunable three-body interactions. We show that taking into account strong three-body forces is *crucial* for understanding the colloidal systems in rotating electric fields, whereas only pairwise interactions do not explain the experimentally-measured interactions or the phase states.

We studied tunable interactions and phase states in monolayer colloidal suspensions affected by in-plane rotating electric fields. With dilute suspensions of silica particles in deionised water, we measured *directly* the tunable pairwise interactions experimentally and compared them to theoretical predictions: The results show excellent agreement, whereas the mapping of the interactions allows to obtain the effective polarisation diameter of particle, determining completely the tunable pairwise and three-body interactions. With dense suspensions, we visualised spinodal decomposition, formation of liquid droplets, and their crystallisation, and obtained the boundaries of different phase states of colloidal clusters. To unravel the role of three-body forces, we compared experimental and MD results for boundaries of gaseous, liquid, and crystalline domains, and discovered that the strong three-body interactions affect significantly the phase states, whereas the phase diagram resembles its 3D counterpart and includes critical and triple points. The tunable electrically-induced pairwise and three-body interactions, as well as contributions of higher orders, can be measured directly with optical tweezers. Corresponding studies are technically more difficult (compared to the methods we used here), but should be performed in the future work to reveal and measure the tunable forces in clusters of different configurations.

Phase diagrams, in particular, reflect possible routes for self-assembly, taking a central place in physics of phase transitions, development of novel materials, and understanding technological processes: The significant change of phase boundaries means that three-body forces should affect kinetics, and mechanisms of phase transitions, as well as transport properties. These problems are largely unstudied on particle-resolved scale and, in particular, in melting scenario. Therefore, one of the key points is that the described system (including the associated experimental methodology and data analysis) constitutes a "laboratory" of three-body interactions allowing to reveal their role in structure, kinetics of phase transitions, and generic behaviour inherent to liquids and solids.

We observed mapping of the phase states in our system onto those of hard disks with dipolar attraction [71] (that is similar to recent magnetic experiments [58]), whereas the pure dipolar attraction *contradicts* the experiments. This seeming paradox is related to the similarity in phase behavior and is completely governed by the effect of three-body forces. This allows us to formulate a problem for future study: How the similarity in phase behaviour is related with transport and elastic properties of matter in different states?

We show that the tunable three-body potential in our system can also be mapped onto that in charged colloids, known as a model system for globular proteins [8], while offering unparalleled flexibility in interaction tuning. Indeed, tunable interactions in our system originate from the bulk polarisation of particles and, thus, are sensitive to their internal structure [75]. Due to this, in addition to the analogy of three-body forces in charged colloids, our approach with rotating electric fields can be generalised to construct anisotropic *tunable patchy-colloid-like* interactions between the particles with anisotropic internal structure, to reproduce sophisticated behaviour of crowded proteins, important for understanding of cellular mechanisms and protein drugs [7, 8]. The same principles could be used for design and self-assembly of novel materials and

colloidal field-assisted 3D printing.

Comparing the system we studied here to previous works on magnetic colloids [52–59], one should note that, in the quasi-static limit, the magnetic and electric systems are described in the same manner. The difference between tunable interactions in electric and magnetic systems arises due to the change in the sign of dielectric or magnetic contrast, respectively [51]: $\varepsilon_P < \varepsilon_S$ and $\lambda < 0$ in our case, whereas for a system of superparamagnetic particles in nonmagnetic solvent (typically used in previous studies, [53–59]) the permittivity of particles is higher than that of the solvent, $\mu_P > \mu_S$ and $\lambda > 0$. On the contrary, at $\varepsilon_P > \varepsilon_S$ and $\lambda > 0$ (e.g., polymethylmethacrylate particles in cyclohexane [75]), we expect to observe the interaction, similar to that in Refs. [52–59]. In the case of magnetic solvent and nonmagnetic particles (in particular, bubbles in magnetic liquids), we expect to observe the results similar to reported here, and the corresponding studies should be performed in future.

In a similar manner, the tunable interactions in both electric and magnetic fields can be engineered with composite structure of colloidal particles [75] and using spatial hodographs of the rotating fields [60]. However, in low-frequency electric fields, the Debey-Falkenhagen effect related to the deformation of ionic clouds in the solvent should arise: In this case, the tunable interactions still remain insufficiently understood, and we leave the corresponding analysis for a future work.

Monolayer systems are inherent to a broad range of functional materials, protein membranes, confined proteins and colloidal particles, epitaxial monolayers, and nanocrystals on graphite. The same framework, as we proposed it here, is also suitable for studies of 3D systems. However, gravitationally-compensated colloidal systems [72] and the spatial hodographs of rotating electric field [60] should be used instead of the in-plane rotating field, to create isotropic tunable interactions. The system should be imaged in bulk, and the same methodology as we propose here, can be applied. However, this case, important for the comparison with bulk liquids and solids, as well as bulk solutions of proteins, stands beyond the scope of our present paper and deserves a separate study.

Overall, results of this work pave the way to reveal the role of strong three-body forces in dislocation dynamics, melting, domain dynamics in polycrystallites, diffusion, gelation and coarsening of gels, interfacial phenomena, kinetics of phase transitions. Therefore, we believe that the present work will stimulate theoretical and experimental studies in related areas of chemical physics, materials science, condensed and soft matter.

Acknowledgments

The authors acknowledge D. Frenkel, K.A. Komarov, A.V. Ivlev, V.N. Ryzhov, and V.V. Brazhkin for useful discussions. E.V.Y., N.P.K., S.A.K., N.A.D., and S.O.Y. acknowledge BMSTU State Assignment for infrastructural support. Electrode system was made at the BMSTU Nanofabrication Facility (FMN Laboratory, FMNS REC, ID 74300). The study was supported by Russian Science Foundation Grant No. 17-19-01691.

Author contributions

E.V.Y. performed experiments; N.P.K. performed MD simulations; N.P.K., S.A.K., N.A.D., P.V.O., and S.O.Y. processed experimental results and MD simulations; M.M.A. and I.A.R. fabricated the electrode system of the experimental cell; E.V.Y., N.P.K., A.V.S., and S.O.Y. analysed and discussed the results; S.O.Y. conceived, designed, directed the study, and wrote the manuscript. All authors reviewed the manuscript.

Bibliography

[1] H.-W. Hammer, A. Nogga, A. Schwenk, Colloquium: Three-body forces: From cold atoms to nuclei, Reviews of Modern Physics 85 (1) (2013) 197–217. doi:10.1103/revmodphys.85.197.
URL https://doi.org/10.1103/revmodphys.85.197

[2] O. A. von Lilienfeld, A. Tkatchenko, Two- and three-body interatomic dispersion energy contributions to binding in molecules and solids, The Journal of Chemical Physics 132 (23) (2010) 234109. doi:10.1063/1.3432765.
URL https://doi.org/10.1063/1.3432765

[3] G. R. Medders, V. Babin, F. Paesani, A critical assessment of two-body and three-body interactions in water, Journal of Chemical Theory and Computation 9 (2) (2013) 1103–1114. doi:10.1021/ct300913g.
URL https://doi.org/10.1021/ct300913g

[4] C. Russ, H. H. von Grünberg, M. Dijkstra, R. van Roij, Three-body forces between charged colloidal particles, Physical Review E 66 (1) (2002) 011402. doi:10.1103/physreve.66.011402.
URL https://doi.org/10.1103/physreve.66.011402

[5] A.-P. Hynninen, M. Dijkstra, R. van Roij, Effect of three-body interactions on the phase behavior of charge-stabilized colloidal suspensions, Physical Review E 69 (6) (2004) 061407. doi:10.1103/physreve.69.061407.
URL https://doi.org/10.1103/physreve.69.061407

[6] D. Reinke, H. Stark, H.-H. von Grünberg, A. B. Schofield, G. Maret, U. Gasser, Noncentral forces in crystals of charged colloids, Physical Review Letters 98 (3) (2007) 038301. doi:10.1103/physrevlett.98.038301.
URL https://doi.org/10.1103/physrevlett.98.038301

[7] N. Skar-Gislinge, M. Ronti, T. Garting, C. Rischel, P. Schurtenberger, E. Zaccarelli, A. Stradner, A colloid approach to self-assembling antibodies, Molecular Pharmaceutics 16 (6) (2019) 2394–2404. doi:10.1021/acs.molpharmaceut.9b00019.
URL https://doi.org/10.1021/acs.molpharmaceut.9b00019

[8] A. Stradner, P. Schurtenberger, Potential and limits of a colloid approach to protein solutions, Soft Matter 16 (2) (2020) 307–323. doi:10.1039/c9sm01953g.
URL https://doi.org/10.1039/c9sm01953g

[9] S. Torquato, Inverse optimization techniques for targeted self-assembly, Soft Matter 5 (6) (2009) 1157. doi:10.1039/b814211b.
URL https://doi.org/10.1039/b814211b

[10] F. H. Stillinger, S. Torquato, Structural degeneracy in pair distance distributions, The Journal of Chemical Physics 150 (20) (2019) 204125. doi:10.1063/1.5096894.
URL https://doi.org/10.1063/1.5096894

[11] A. Fernandez-Nieves, A. M. Puertas, Fluids, colloids, and soft materials: an introduction to soft matter physics, Wiley, 2016.

[12] A. Ivlev, H. Löwen, G. Morfill, C. P. Royall, Complex plasmas and Colloidal dispersions: particle-resolved studies of classical liquids and solids (Series in soft condensed matter), Singapore: Word Scientific, 2012.

[13] H. Löwen, Melting, freezing and colloidal suspensions, Phys. Rep. 237 (5) (1994) 249 – 324. doi:10.1016/0370-1573(94)90017-5.
URL http://www.sciencedirect.com/science/article/pii/0370157394900175

[14] B. Li, D. Zhou, Y. Han, Assembly and phase transitions of colloidal crystals, Nature Reviews Materials 1 (2) (2016) 15011. doi:10.1038/natrevmats.2015.11.
URL https://doi.org/10.1038/natrevmats.2015.11

[15] A. M. Alsayed, Premelting at defects within bulk colloidal crystals, Science 309 (5738) (2005) 1207–1210. doi:10.1126/science.1112399.
URL https://doi.org/10.1126/science.1112399

[16] J. Taffs, S. R. Williams, H. Tanaka, C. P. Royall, Structure and kinetics in the freezing of nearly hard spheres, Soft Matter 9 (1) (2013) 297–305. doi:10.1039/c2sm26473k.
URL https://doi.org/10.1039/c2sm26473k

[17] K. Zahn, R. Lenke, G. Maret, Two-stage melting of paramagnetic colloidal crystals in two dimensions, Physical Review Letters 82 (13) (1999) 2721–2724. doi:10.1103/physrevlett.82.2721.
URL https://doi.org/10.1103/physrevlett.82.2721

[18] K. Zahn, G. Maret, Dynamic criteria for melting in two dimensions, Physical Review Letters 85 (17) (2000) 3656–3659. doi:10.1103/physrevlett.85.3656.
URL https://doi.org/10.1103/physrevlett.85.3656

[19] J. Sprakel, A. Zaccone, F. Spaepen, P. Schall, D. A. Weitz, Direct observation of entropic stabilization of bcc crystals near melting, Physical Review Letters 118 (8) (2017) 088003. doi:10.1103/physrevlett.118.088003.
URL https://doi.org/10.1103/physrevlett.118.088003

[20] D. Paloli, P. S. Mohanty, J. J. Crassous, E. Zaccarelli, P. Schurtenberger, Fluid-solid transitions in soft-repulsive colloids, Soft Matter 9 (11) (2013) 3000. doi:10.1039/c2sm27654b.
URL https://doi.org/10.1039/c2sm27654b

[21] Z. Wang, F. Wang, Y. Peng, Z. Zheng, Y. Han, Imaging the homogeneous nucleation during the melting of superheated colloidal crystals, Science 338 (6103) (2012) 87–90. doi:10.1126/science.1224763.
URL https://doi.org/10.1126/science.1224763

[22] C. P. Royall, M. E. Leunissen, A.-P. Hynninen, M. Dijkstra, A. van Blaaderen, Re-entrant melting and freezing in a model system of charged colloids, The Journal of Chemical Physics 124 (24) (2006) 244706. doi:10.1063/1.2189850.
URL https://doi.org/10.1063/1.2189850

[23] A. Yethiraj, A. van Blaaderen, A colloidal model system with an interaction tunable from hard sphere to soft and dipolar, Nature 421 (6922) (2003) 513–517. doi:10.1038/nature01328.
URL https://doi.org/10.1038/nature01328

[24] Y. Peng, F. Wang, Z. Wang, A. M. Alsayed, Z. Zhang, A. G. Yodh, Y. Han, Two-step nucleation mechanism in solid-solid phase transitions, Nature Materials 14 (1) (2014) 101–108. doi:10.1038/nmat4083.
URL https://doi.org/10.1038/nmat4083

[25] C. P. Royall, D. G. A. L. Aarts, H. Tanaka, Bridging length scales in colloidal liquids and interfaces from near-critical divergence to single particles, Nature Physics 3 (9) (2007) 636–640. doi:10.1038/nphys679.
URL https://doi.org/10.1038/nphys679

[26] I. Zhang, C. P. Royall, M. A. Faers, P. Bartlett, Phase separation dynamics in colloid–polymer mixtures: the effect of interaction range, Soft Matter 9 (6) (2013) 2076. doi:10.1039/c2sm27119b.
URL https://doi.org/10.1039/c2sm27119b

[27] B. Li, X. Xiao, S. Wang, W. Wen, Z. Wang, Real-space mapping of the two-dimensional phase diagrams in attractive colloidal systems, Physical Review X 9 (3) (2019) 031032. doi:10.1103/physrevx.9.031032.
URL https://doi.org/10.1103/physrevx.9.031032

[28] W. N. Everett, H.-J. Wu, S. G. Anekal, H.-J. Sue, M. A. Bevan, Diffusing colloidal probes of protein and synthetic macromolecule interactions, Biophysical Journal 92 (3) (2007) 1005–1013. doi:10.1529/biophysj.106.094102.
URL https://doi.org/10.1529/biophysj.106.094102

[29] C. Zhu, S. Liang, E. Song, Y. Zhou, W. Wang, F. Shan, Y. Shi, C. Hao, K. Yin, T. Zhang, J. Liu, H. Zheng, L. Sun, In-situ liquid cell transmission electron microscopy investigation on oriented attachment of gold nanoparticles, Nature Communications 9 (1) (2018) 421. doi:10.1038/s41467-018-02925-6.
URL https://doi.org/10.1038/s41467-018-02925-6

[30] F. Martínez-Pedrero, J. Benet, J. E. F. Rubio, E. Sanz, R. G. Rubio, F. Ortega, Field-induced sublimation in perfect two-dimensional colloidal crystals, Physical Review E 89 (1) (2014) 012306. doi:10.1103/physreve.89.012306.
URL https://doi.org/10.1103/physreve.89.012306

[31] E. R. Weeks, J. C. Crocker, A. C. Levitt, A. Schofield, D. A. Weitz, Three-dimensional direct imaging of structural relaxation near the colloidal glass transition, Science 287 (5453) (2000) 627–631. doi:10.1126/science.287.5453.627.
URL https://doi.org/10.1126/science.287.5453.627

[32] A. I. Campbell, V. J. Anderson, J. S. van Duijneveldt, P. Bartlett, Dynamical arrest in attractive colloids: The effect of long-range repulsion, Physical Review Letters 94 (20) (2005) 208301. doi:10.1103/physrevlett.94.208301.
URL https://doi.org/10.1103/physrevlett.94.208301

[33] A. Zaccone, J. J. Crassous, M. Ballauff, Colloidal gelation with variable attraction energy, The Journal of Chemical Physics 138 (10) (2013) 104908. doi:10.1063/1.4794695.
URL https://doi.org/10.1063/1.4794695

[34] C. P. Royall, S. R. Williams, The role of local structure in dynamical arrest, Physics Reports 560 (2015) 1–75. doi:10.1016/j.physrep.2014.11.004.
URL https://doi.org/10.1016/j.physrep.2014.11.004

[35] A. Yethiraj, J. Thijssen, A. Wouterse, A. van Blaaderen, Large-area electric-field-induced colloidal single crystals for photonic applications, Advanced Materials 16 (7) (2004) 596–600. doi:10.1002/adma.200306192.
URL https://doi.org/10.1002/adma.200306192

[36] V. Sharma, Q. Yan, C. Wong, W. C. Carter, Y.-M. Chiang, Controlled and rapid ordering of oppositely charged colloidal particles, Journal of Colloid and Interface Science 333 (1) (2009) 230–236. doi:10.1016/j.jcis.2009.01.047.
URL https://doi.org/10.1016/j.jcis.2009.01.047

[37] C. Zhu, A. J. Pascall, N. Dudukovic, M. A. Worsley, J. D. Kuntz, E. B. Duoss, C. M. Spadaccini, Colloidal materials for 3d printing, Annual Review of Chemical and Biomolecular Engineering 10 (1) (2019) 17–42. doi:10.1146/annurev-chembioeng-060718-030133.
URL https://doi.org/10.1146/annurev-chembioeng-060718-030133

[38] J. J. Martin, B. E. Fiore, R. M. Erb, Designing bioinspired composite reinforcement architectures via 3d magnetic printing, Nature Communications 6 (1) (2015) 8641. doi:10.1038/ncomms9641.
URL https://doi.org/10.1038/ncomms9641

[39] Y. Yang, X. Li, M. Chu, H. Sun, J. Jin, K. Yu, Q. Wang, Q. Zhou, Y. Chen, Electrically assisted 3d printing of nacre-inspired structures with self-sensing capability, Science Advances 5 (4) (2019) eaau9490. doi:10.1126/sciadv.aau9490.
URL https://doi.org/10.1126/sciadv.aau9490

[40] D. Du, M. Doxastakis, E. Hilou, S. L. Biswal, Two-dimensional melting of colloids with long-range attractive interactions, Soft Matter 13 (8) (2017) 1548–1553. doi:10.1039/c6sm02131j.
URL https://doi.org/10.1039/c6sm02131j

[41] Y. Yuan, M. Tasinkevych, I. I. Smalyukh, Colloidal interactions and unusual crystallization versus de-mixing of elastic multipoles formed by gold mesoflowers, Nature Communications 11 (1) (2020) 188. doi:10.1038/s41467-019-14031-2.

URL https://doi.org/10.1038/s41467-019-14031-2
[42] O. D. Velev, S. Gangwal, D. N. Petsev, Particle-localized AC and DC manipulation and electrokinetics, Annual Reports Section "C" (Physical Chemistry) 105 (2009) 213. doi:10.1039/b803015b.
URL https://doi.org/10.1039/b803015b
[43] K.-Q. Zhang, X. Y. Liu, Controlled formation of colloidal structures by an alternating electric field and its mechanisms, The Journal of Chemical Physics 130 (18) (2009) 184901. doi:10.1063/1.3127383.
URL https://doi.org/10.1063/1.3127383
[44] M. Mittal, P. P. Lele, E. W. Kaler, E. M. Furst, Polarization and interactions of colloidal particles in ac electric fields, The Journal of Chemical Physics 129 (6) (2008) 064513. doi:10.1063/1.2969103.
URL https://doi.org/10.1063/1.2969103
[45] X. Tang, B. Rupp, Y. Yang, T. D. Edwards, M. A. Grover, M. A. Bevan, Optimal feedback controlled assembly of perfect crystals, ACS Nano 10 (7) (2016) 6791–6798. doi:10.1021/acsnano.6b02400.
URL https://doi.org/10.1021/acsnano.6b02400
[46] D. R. E. Snoswell, C. L. Bower, P. Ivanov, M. J. Cryan, J. G. Rarity, B. Vincent, Dynamic control of lattice spacing within colloidal crystals, New Journal of Physics 8 (11) (2006) 267–267. doi:10.1088/1367-2630/8/11/267.
URL https://doi.org/10.1088/1367-2630/8/11/267
[47] N. Elsner, C. P. Royall, B. Vincent, D. R. E. Snoswell, Simple models for two-dimensional tunable colloidal crystals in rotating ac electric fields, The Journal of Chemical Physics 130 (15) (2009) 154901. doi:10.1063/1.3115641.
URL https://doi.org/10.1063/1.3115641
[48] J. J. Juárez, S. E. Feicht, M. A. Bevan, Electric field mediated assembly of three dimensional equilibrium colloidal crystals, Soft Matter 8 (1) (2012) 94–103. doi:10.1039/c1sm06414b.
URL https://doi.org/10.1039/c1sm06414b
[49] E. V. Yakovlev, K. A. Komarov, K. I. Zaytsev, N. P. Kryuchkov, K. I. Koshelev, A. K. Zotov, D. A. Shelestov, V. L. Tolstoguzov, V. N. Kurlov, A. V. Ivlev, S. O. Yurchenko, Tunable two-dimensional assembly of colloidal particles in rotating electric fields, Scientific Reports 7 (1) (2017) 13727. doi:10.1038/s41598-017-14001-y.
URL https://doi.org/10.1038/s41598-017-14001-y
[50] K. A. Komarov, N. P. Kryuchkov, S. O. Yurchenko, Tunable interactions between particles in conically rotating electric fields, Soft Matter 14 (47) (2018) 9657–9674. doi:10.1039/c8sm01538d.
URL https://doi.org/10.1039/c8sm01538d
[51] K. A. Komarov, A. V. Yarkov, S. O. Yurchenko, Diagrammatic method for tunable interactions in colloidal suspensions in rotating electric or magnetic fields, The Journal of Chemical Physics 151 (24) (2019) 244103. doi:10.1063/1.5131255.
URL https://doi.org/10.1063/1.5131255
[52] B. A. Grzybowski, H. A. Stone, G. M. Whitesides, Dynamic self-assembly of magnetized, millimetre-sized objects rotating at a liquid–air interface, Nature 405 (6790) (2000) 1033–1036. doi:10.1038/35016528.
URL https://doi.org/10.1038/35016528
[53] N. Osterman, I. Poberaj, J. Dobnikar, D. Frenkel, P. Ziherl, D. Babić, Field-induced self-assembly of suspended colloidal membranes, Physical Review Letters 103 (22) (2009) 228301. doi:10.1103/physrevlett.103.228301.
URL https://doi.org/10.1103/physrevlett.103.228301
[54] D. Du, D. Li, M. Thakur, S. L. Biswal, Generating an in situ tunable interaction potential for probing 2-d colloidal phase behavior, Soft Matter 9 (29) (2013) 6867. doi:10.1039/c3sm27620a.
URL https://doi.org/10.1039/c3sm27620a
[55] J. E. Martin, A. Snezhko, Driving self-assembly and emergent dynamics in colloidal suspensions by time-dependent magnetic fields, Reports on Progress in Physics 76 (12) (2013) 126601. doi:10.1088/0034-4885/76/12/126601.
URL https://doi.org/10.1088/0034-4885/76/12/126601
[56] K. Müller, N. Osterman, D. Babič, C. N. Likos, J. Dobnikar, A. Nikoubashman, Pattern formation and coarse-graining in two-dimensional colloids driven by multiaxial magnetic fields, Langmuir 30 (18) (2014) 5088–5096. doi:10.1021/la500896e.
URL https://doi.org/10.1021/la500896e
[57] A. T. Pham, Y. Zhuang, P. Detwiler, J. E. S. Socolar, P. Charbonneau, B. B. Yellen, Phase diagram and aggregation dynamics of a monolayer of paramagnetic colloids, Physical Review E 95 (5) (2017) 052607. doi:10.1103/physreve.95.052607.
URL https://doi.org/10.1103/physreve.95.052607
[58] E. Hilou, K. Joshi, S. L. Biswal, Characterizing the spatiotemporal evolution of paramagnetic colloids in time-varying magnetic fields with minkowski functionals, Soft Matter 16 (38) (2020) 8799–8805. doi:10.1039/d0sm01100b.
URL https://doi.org/10.1039/d0sm01100b
[59] I. M. Kulić, M. L. Kulić, Self-assembly of colloidal superstructures in coherently fluctuating fields, Physical Review Letters 111 (19). doi:10.1103/physrevlett.111.198301.
URL https://doi.org/10.1103/physrevlett.111.198301
[60] K. A. Komarov, S. O. Yurchenko, Colloids in rotating electric and magnetic fields: designing tunable interactions with spatial field hodographs, Soft Matter 16 (35) (2020) 8155–8168. doi:10.1039/d0sm01046d.
URL https://doi.org/10.1039/d0sm01046d
[61] E. Hilou, D. Du, S. Kuei, S. L. Biswal, Interfacial energetics of two-dimensional colloidal clusters generated with a tunable anharmonic interaction potential, Physical Review Materials 2 (2) (2018) 025602. doi:10.1103/physrevmaterials.2.025602.
URL https://doi.org/10.1103/physrevmaterials.2.025602
[62] S. H. Klapp, Collective dynamics of dipolar and multipolar colloids: From passive to active systems, Current Opinion in Colloid & Interface Science 21 (2016) 76–85. doi:10.1016/j.cocis.2016.01.004.
URL https://doi.org/10.1016/j.cocis.2016.01.004
[63] R. Soheilian, H. Abdi, C. E. Maloney, R. M. Erb, Assembling particle clusters with incoherent 3d magnetic fields, Journal of Colloid and Interface Science 513 (2018) 400–408. doi:10.1016/j.jcis.2017.11.036.
URL https://doi.org/10.1016/j.jcis.2017.11.036
[64] F. Martínez-Pedrero, F. Ortega, J. Codina, C. Calero, R. G. Rubio, Controlled disassembly of colloidal aggregates confined at fluid interfaces using magnetic dipolar interactions, Journal of Colloid and Interface Science 560 (2020) 388–397. doi:10.1016/j.jcis.2019.10.008.
URL https://doi.org/10.1016/j.jcis.2019.10.008
[65] B. M. Axilrod, E. Teller, Interaction of the van der waals type between three atoms, The Journal of Chemical Physics 11 (6) (1943) 299–300. doi:10.1063/1.1723844.
URL https://doi.org/10.1063/1.1723844
[66] J. A. Barker, D. Henderson, What is "liquid"? understanding the states of matter, Reviews of Modern Physics 48 (4) (1976) 587–671. doi:10.1103/revmodphys.48.587.
URL https://doi.org/10.1103/revmodphys.48.587
[67] P. R. ten Wolde, D. Frenkel, Enhancement of protein crystal nucleation by critical density fluctuations, Science 277 (5334) (1997) 1975–1978. doi:10.1126/science.277.5334.1975.
URL https://doi.org/10.1126/science.277.5334.1975
[68] E. Luijten, H. W. J. Blöte, Boundary between long-range and short-range critical behavior in systems with algebraic interactions, Physical Review Letters 89 (2) (2002) 025703. doi:10.1103/physrevlett.89.025703.
URL https://doi.org/10.1103/physrevlett.89.025703
[69] See Supporting Information (URL).
[70] P. V. Ovcharov, N. P. Kryuchkov, K. I. Zaytsev, S. O. Yurchenko, Particle-resolved phase identification in two-dimensional condensable systems, The Journal of Physical Chemistry C 121 (48) (2017) 26860–26868. doi:10.1021/acs.jpcc.7b09317.
URL https://doi.org/10.1021/acs.jpcc.7b09317
[71] N. P. Kryuchkov, F. Smallenburg, A. V. Ivlev, S. O. Yurchenko,

H. Löwen, Phase diagram of two-dimensional colloids with yukawa repulsion and dipolar attraction, The Journal of Chemical Physics 150 (10) (2019) 104903. doi:10.1063/1.5082785.
URL https://doi.org/10.1063/1.5082785

[72] E. V. Yakovlev, M. Chaudhuri, N. P. Kryuchkov, P. V. Ovcharov, A. V. Sapelkin, S. O. Yurchenko, Experimental validation of interpolation method for pair correlations in model crystals, The Journal of Chemical Physics 151 (11) (2019) 114502. doi:10.1063/1.5116176.
URL https://doi.org/10.1063/1.5116176

[73] D. Frenkel, B. Smit, Understanding Molecular Simulation: From Algorithms to Applications, Academic Press, 2001.

[74] C. P. Royall, W. C. K. Poon, E. R. Weeks, In search of colloidal hard spheres, Soft Matter 9 (1) (2013) 17–27. doi:10.1039/c2sm26245b.
URL https://doi.org/10.1039/c2sm26245b

[75] K. A. Komarov, V. N. Mantsevich, S. O. Yurchenko, Core-shell particles in rotating electric and magnetic fields: Designing tunable interactions via particle engineering, The Journal of Chemical Physics 155 (8) (2021) 084903. doi:10.1063/5.0055566.
URL https://doi.org/10.1063/5.0055566